Nonlin. Processes Geophys. Discuss., 1, 1365–1379, 2014
www.nonlin-processes-geophys-discuss.net/1/1365/2014/
doi:10.5194/npgd-1-1365-2014

Nonlinear Processes in Geophysics
Discussions
Open Access

Multifractal analysis of mercury inclusions in quartz by X-ray computed tomography

T. Shibata[1,2], **T. Maruoka**[3], **and T. Echigo**[4]

[1]Geological Survey of Hokkaido, Hokkaido Research Organization, N19 W12, Kita-ku, Sapporo, Hokkaido 060-0819, Japan
[2]Institute for Geothermal Sciences, Graduate School of Science, Kyoto University, Noguchibaru 3088, Beppu, Oita 874-0903, Japan
[3]Graduate School of Life and Environmental Sciences, University of Tsukuba, Tennodai 1-1-1, Tsukuba, Ibaraki 305-8572, Japan
[4]Department of Natural Science, Faculty of Education, Shiga University, Hiratsu 2-5-1, Otsu, Shiga 520-0862, Japan

Received: 6 June 2014 – Accepted: 16 July 2014 – Published: 14 August 2014

Correspondence to: T. Shibata (swn05-toshibat@bep.vgs.kyoto-u.ac.jp)

Published by Copernicus Publications on behalf of the European Geosciences Union & the American Geophysical Union.

Abstract

In order to refine our understanding how fluid inclusions were trapped in the host minerals, we non-destructively observed mercury inclusions (liquid Hg^0) in quartz samples using X-ray computed tomography (CT) technique. The X-ray CT apparatus can observe internal structures of the samples and give cross-sectional images from the transmission of the X-rays through the samples. From the cross-sectional images, we obtained three-dimensional spatial distributions of mercury inclusions, and quantitatively analyzed them using fractal and multifractal methods. Although the samples were from different mines, the resultant fractal dimensions were about 1.7 for the samples. The fractal dimensions were also close to those predicted by diffusion-limited aggregation models and percolation theory, which are controlled by the irreversible kinetics. Then, the mercury-bearing fluids were not primary fluid inclusions, but migrated into the pre-existing cracks of quartz crystals by diffusion processes.

1 Introduction

Fluid inclusions in minerals record important clues to past geologic processes that the host minerals were subjected to. We can obtain information on physical and chemical factors, such as the pressure, temperature, density and composition of the fluids, from the fluid inclusions in minerals (e.g., Takeuchi, 1975; Roedder, 1984). However, studying fluid inclusions poses many difficulties for precise analysis because of the high mobility and evaporation involved. Therefore, non-destructive analytical methods, such as micro-Raman spectroscopy (Burke, 2001; Frezzotti et al., 2012), synchrotron-radiation X-ray fluorescence (SR-XRF) (Schmidt and Rickers, 2003; Tsuchiyama et al., 2009) and proton-induced X-ray emission (PIXE) (Kurosawa et al., 2003), have been developed for the chemical analysis of individual fluid inclusions in minerals. It is also necessary to observe the spatial distribution of different fluid inclusion populations within a mineral grain to establish their paragenetic succession relative to the mineral

NPGD
1, 1365–1379, 2014

formation (i.e., primary, secondary and pseudo-secondary inclusions) (e.g., Takeuchi, 1975; Roedder, 1984). X-ray computed tomography (CT) is a non-destructive analytical method, and is one of the effective methods for observing the spatial distribution of fluid inclusions.

The X-ray CT technique, which was originally developed to obtain cross-sectional images, has recently been applied to minerals and rocks, and has opened up a new approach for resolving their internal and three-dimensional structures (Martínez et al., 2010). Although the internal structures of rocks are generally heterogeneous and complex, they have been successfully characterized using fractal geometry (Pasadas et al., 2009; Martínez et al., 2010). In particular, fractal and multifractal analysis, described by Mandelbrot (1982) and Takayasu (1986), was developed for the quantitative analysis of the patterns of irregular shapes and complicated phenomena. Fractal and multifractal analysis has been used in several geochemical studies to understand structures observed in sediments and soils, such as pore shapes and water distribution (Bird et al., 2006; Pasadas et al., 2009; Ferreiro and Vázquez, 2010; Martínez et al., 2010; Xie et al., 2010). Here we observed mercury inclusions (liquid Hg^0) in quartz by the X-ray CT, and quantitatively analyzed their three-dimensional distribution using fractal and multifractal methods.

2 Materials and methods

X-ray CT can be used for non-destructively analyzing the internal structures of objective materials. Therefore, it is suitable for samples, including fluids, that disappear if a destructive method is used. We examined a quartz crystal from San Benito, California, USA and another from Itomuka, Hokkaido, Japan (sized 2 cm × 5 cm × 7 cm and 4 cm × 5 cm × 6 cm, respectively). In these mines, native mercury (liquid Hg^0) occurs as droplets in the quartz crystals, formed by hydrothermal fluids associated with Neogene/Quaternary volcanic activities (Sugimoto et al., 1972; Harada and Haritani, 1984; Peabody and Einaudy, 1992; Dunning et al., 2005). The samples examined are

NPGD
1, 1365–1379, 2014

idiomorphic and polycrystalline quartz, and contain visible clusters and/or films of 1–2 mm mercury inclusions.

We used a microfocus X-ray CT system (SMX-225CT; Shimazu Corp., Kyoto, Japan), which can distinguish fluid inclusion of mercury (13.59 g cm^{-3}) from the quartz matrix (2.65 g cm^{-3}) based on the difference between their densities. This apparatus forms cross-sectional images by the transmission of the X-ray through the samples. The nominal resolution of the cross-section thickness and the interval between the cross-sections were 0.120 and 0.073 mm, respectively. The cross-sectional images were composed of a 512 pixel × 512 pixel array that corresponded to an area of 9.88 cm × 9.88 cm (therefore, one pixel corresponds to an area of 0.193 mm × 0.193 mm). One of the cross-sectional images is shown in Fig. 1. The grey circle in Fig. 1a represents the field of view for the X-ray CT system, and the irregular region marked in the center of the field of view represents the quartz. The region outside of the quartz is air, containing no solid matter. The white dots represent mercury inclusions in the quartz.

The sequenced cross-sectional images were reconstructed and incorporated onto the images of each quartz crystal using the Image Processing and Analysis software in Java-ImageJ (Rasband, 1997–2011; Abramoff et al., 2004). Areas of mercury inclusions in the quartz were extracted from the images using threshold filtering. The spatial distributions of mercury inclusions analyzed by fractal and multifractal theory.

3 Fractal and multifractal analysis

Fractal and multifractal behavior is common in nature, and that the spatial distributions of mercury inclusions have fractal and multifractal shapes. Because a fractal shape typically has a self-similar structure and scale-free properties, the degree of distribution of the shape follows a power law in the form

$$N(r) \propto r^{-D}, \quad (1)$$

NPGD
1, 1365–1379, 2014

where $N(r)$ is the number of objects, r is the scale and D is the capacity (fractal) dimension. The capacity dimension, D, which is generally estimated using a box-counting technique, is defined by the relationship between the scaling properties of the distribution by covering it with boxes of size, r, and counting the number of boxes containing $N(r)$, as follows:

$$D = -\lim_{r\to 0} \frac{\log N(r)}{\log r}. \quad (2)$$

Then, the capacity dimension can be approximately determined as the negative slope of $\log N(r)$ vs. $\log r$. Although the capacity dimension is a fundamental and quantitative parameter of the fractal, the dimension cannot completely describe complex and heterogeneous structures. Therefore, we applied the multifractal theory to analyze the spatial distribution of the mercury inclusions, as described below.

The multifractal theory can be characterized on the basis of the generalized dimensions of the qth order moment of a distribution, D_q. The generalized dimensions, D_q, can be defined by the function

$$D_q = \lim_{r\to 0} \frac{\log \sum_i P_i(r)^q}{(q-1)\log r}, \quad (3)$$

where $P_i(r)^q$ is the probability within the ith region of a measured quantity varying with scale r (Takayasu, 1986). The generalized dimension, D_q, can be rewritten with the singularity exponent, α, and the generalized fractal dimension, $f(\alpha)$, as the equation

$$D_q = \frac{q\alpha(q) - f(\alpha(q))}{(q-1)}. \quad (4)$$

When we can obtain the generalized dimension, D_q, from experiments, the singularity exponent, α, and the generalized fractal dimension, $f(\alpha)$, can be estimated using the following relationships

$$\alpha(q) = \frac{\mathrm{d}}{\mathrm{d}q}(q-1)D_q \quad (5)$$

NPGD
1, 1365–1379, 2014

and

$$f(\alpha(q)) = q\alpha(q) - (q-1)D_q. \quad (6)$$

The singularity exponent, α, is characterized by scaling in the local region, and quantifies the degree of regularity in the region. The sub-sets with a local scaling exponent of α form the fractal distribution, and its fractal dimension can be viewed as the generalized fractal dimension, $f(\alpha)$. The multifractal theory allows the characterization of complex phenomena in a fully quantitative manner for both temporal and spatial variations.

4 Results and discussion

The mercury inclusions in the host quartz crystals seemed to be clustered, and were ramified peripherally and randomly so that the clusters resembled dendritic structures. There was no natural scale length in the structures at scales much larger than the particle size, and a self-similar structure was formed. We analyzed the mercury inclusion clusters in the quartz samples using the above equations. We estimated the relationship between the logarithm of the number of objects, $\log N(r)$, and the logarithm of the box-size, $\log r$, using the box-counting technique (Fig. 2). The capacity dimensions, D, were found to be 1.70 and 1.71 for the San Benito and Itomuka samples, respectively, from the slopes of the relationships shown in Fig. 2. The capacity dimensions generally indicate major cluster shapes, for example lines and surfaces have the values $D = 1$ and $D = 2$, respectively. The obtained dimensions show that the mercury inclusion clusters found in the quartz samples were more complex than lines but were not entirely surfaces. The San Benito and Itomuka mercury deposits occurred in altered rocks, which would have been formed by hydrothermal fluids in the Neogene/Quaternary age (Dunning et al., 2005; Sugimoto et al., 1972). Both samples tested here would have been subjected to similar geological conditions at the same age, although they were from different deposits.

NPGD
1, 1365–1379, 2014

Several studies have been performed using fractal geometry, which is controlled by the irreversible kinetic processes such as diffusion, aggregation and percolation. These processes have been described by the diffusion-limited aggregation (DLA) and percolation mechanism, which involves Brownian particle motion (e.g., Witten and Sander, 1983; Meakin, 1985; Zheng et al., 1998; Stauffer, 1979; Hunt and Ewing, 2009). Based on the DLA models, the fractal dimension, D, is predicted to be equal to $(d^2+1)/(d+1)$, where d is the spatial dimensionality (Muthukumar, 1983). For a two- and three-dimensional system D should be 5/3 (1.66) and 5/2 (2.5), respectively. Also, percolation theory shows that the fractal dimensions are 1.89 and 2.54 in two- and three-dimensional systems D, respectively. Estimated fractal dimensions of the mercury inclusions in our quartz samples from San Benito and Itomuka are similar to these obtained by DLA models and percolation theory for two-dimensional system. This suggests that mercury-bearing fluids would imply information on paragenetic succession of mineral and crystallization processes.

Dunning et al. (2005) observed deposit of San Benito sample in geology and mineralogy, and deduced that quartz is formed in earlier than mercury is done. Itomuka sample is also the same formation and age as San Benito sample, although they are from different deposits. From the fractal dimensions and geological deduction, fluids of mercury inclusions would be captured into quartz after its crystallization process. Therefore, the mercury-bearing fluids were not the primary fluid inclusions, but were trapped in cracks that already existed in the quartz samples.

Multifractal analysis allowed us to examine the complex signature of the mercury inclusion clusters more quantitatively. We obtained three sets of multifractal parameters, α, $f(\alpha)$ and D_q. Figure 3 shows multifractal spectra in which the generalized fractal dimensions, $f(\alpha)$, are plotted against the singularity exponent, α. Multifractal spectra generally show parabolic curves that are concave downwards, and the curve maxima occur at $q = 0$, at which point $f(\alpha)$ in the San Benito and Itomuka samples corresponded to the capacity dimensions of 1.70 and 1.71, respectively. The parabola of both samples had similar curves, but the width of the parabola was larger

NPGD
1, 1365–1379, 2014

for the San Benito sample than for the Itomuka sample. The San Benito sample had more fractal structure patterns than the Itomuka sample, because wider curves reflect more heterogeneous structures in the mercury inclusion distributions.

Figure 4 shows the difference between the fractal dimension distributions in the samples, and the relationships between the generalized dimensions, D_q, and the order moments, q. In general, D_q dimensions increase with decreasing q moments. In Fig. 4, the curves for both quartz samples are similar. The q moments are interpreted as a parameter of the inclusion distribution probability densities, i.e., low-q implies a low distribution density and high-q implies a high density. The D_q dimensions at low-q moments in the samples were 2.3–2.7, indicating that the distribution of surface and spatial structures were scarce. However, the D_q dimensions at high-q moments were 1.0–1.3, indicating that linear configurations were common. Consequently, mercury inclusions ramified like a dendritical structure. This implies that mercury-bearing fluids migrated linearly into the quartz sample cracks and then expanded to form surface plane and spatial figurations.

5 Conclusions

We proposed to analyze of mercury inclusions in quartz samples using in situ X-ray computed tomography (CT). The X-ray CT apparatus allows the internal structures of the quartz samples to be analyzed non-destructively, and therefore, mercury inclusions are to be retained in the quartz throughout the experiment. We performed X-ray CT measurements on two quartz samples, one from San Benito, California, USA and one from Itomuka, Hokkaido, Japan, both of which contain visible mercury inclusions. We obtained the spatial distributions of the mercury inclusions based on sequenced X-ray cross-sectional images. Spatial distributions can be explored quantitatively using fractal and multifractal theory. We showed the fractal dimensions, α–$f(\alpha)$, multifractal spectra and the relationship between q and D_q. The mercury inclusions trapped in the quartz samples had similar distribution signatures, even though the quartz samples were from

NPGD
1, 1365–1379, 2014

different mines. In addition, the fractal dimensions were close to those obtained by diffusion-limited aggregation DLA models and percolation theory for two-dimensional system. The similar mercury inclusion signatures correspond to the samples being formed during a process of diffusion into pre-existing cracks in the quartz. After the formation of crystalline quartz, the mercury-bearing fluids probably migrated into pre-existing cracks in the quartz crystals, and native mercury was lodged in the cavities.

Author contribution. T. Shibata designed the study, T. Maruoka performed the X-ray CT measurements and T. Echigo prepared samples. T. Maruoka. and T. Echigo gave technical supports and conceptual advice, and T. Shibata prepared the manuscript with contributions from all co-authors.

Acknowledgements. This study was financially supported in part by Grant-in-Aid for Scientific Research from the Ministry of Education, Science and Culture, Japan (18251002, PD20–1531, 23840049 and 24101010) and the Fukada Geological Institute (2011#7). The authors wish to thank the Editor A. G. Hunt for helpful suggestions in the preparation of this manuscript.

References

Abramoff, M. D., Magalhaes, P. J., and Ram, S. J.: Image processing with ImageJ, Biophotonics International, 11, 36–42, 2004.

Bird, N., Díaz, M. C., Saa, A., and Tarquis, A. M.: Fractal and multifractal analysis of pore-scale images of soil, J. Hydrol., 322, 211–219, 2006.

Burke, E. A. J.: Raman microspectrometry of fluid inclusions, Lithos, 55, 139–158, 2001.

Dunning, G. E., Hadley, T. A., Magnasco, J., Christy, A. G., and Cooper Jr., J. F.: The clear Creek mine, San Benito county, California: a unique mercury locality, Mineral. Rec., 36, 337–363, 2005.

Ferreiro, J. P. and Vázquez, E. V.: Multifractal analysis of Hg pore size distributions in soils with contrasting structural stability, Geoderma, 160, 64–73, 2010.

Frezzotti, M. L., Tecce, F., and Casagli, A.: Raman spectrometry for fluid inclusion analysis, J. Geochem. Explor., 122, 1–20, 2012.

Harada, J. and Haritani, Y.: Minerals in Hokkaido, Geological Survey of Hokkaido, Sapporo, 1984.

NPGD

1, 1365–1379, 2014

Hunt, A. and Ewing, R.: Percolation Theory for Flow in Porous Media, 2nd edn., Lecture Notes in Physics 711, Springer, Berlin, 2009.
Kurosawa, M., Shimano, S., Ishii, S., Shima, K., and Kato, T.: Quantitative trace element analysis of single fluid inclusions by proton-induced X-ray emission (PIXE): application to fluid inclusions in hydrothermal quartz, Geochim. Cosmochim. Ac., 67, 4337–4352, 2003.
Mandelbrot, B. B.: The Fractal Geometry of Nature, W. H. Freeman, San Francisco, 1982.
Martínez, F. S. J., Martín, M. A., Caniego, F. J., Tuller, M., Guber, A., Pachepsky, Y., and Carcía-Gutiérrez, C.: Multifractal analysis of discretized X-ray CT images for the characterization of soil macropore structures, Geoderma, 156, 32–42, 2010.
Meakin, P.: The structure of two-dimensional Witten-Sander aggregates, J. Phys. A-Math. Gen., 18, L661–L666, 1985.
Muthukumar, M.: Mean-field theory for diffusion-limited cluster formation, Phys. Rev. Lett., 50, 839–842, 1983.
Peabody, C. E. and Einaudy, M.: Origin of petroleum and mercury in the Culver-Baer cinnabar deposit, Mayacmas district, California, Econ. Geol., 87, 1078–1103, 1992.
Posadas, A., Quiroz, R., Tannús, A., Crestana, S., and Vaz, C. M.: Characterizing water fingering phenomena in soils using magnetic resonance imaging and multifractal theory, Nonlin. Processes Geophys., 16, 159–168, doi:10.5194/npg-16-159-2009, 2009.
Rasband, W. A.: ImageJ, US National Institutes of Health, Bethesda, Maryland, USA, available at: imagej.nih.gov/ij/, last access: July 2014, 1997–2011.
Roedder, E.: Fluid inclusions, in: Reviews in Mineralogy, Mineralogical Society of America, 12, 1–646, 1984.
Schmidt, C. and Rickers, K.: In-situ determination of mineral solubilities in fluids using a hydrothermal diamond-anvil cell and SR-XRF: solubility of AgCl in water, Am. Mineral., 88, 288–292, 2003.
Stauffer, D.: Scaling theory of percolation clusters, Phys. Rep., 54, 1–74, 1979.
Sugimoto, R., Fujiwara, T., and Futamase, K.: Mercury ore deposits of Itomuka district, Abashiri province, Hokkaido, Report of the Geological Survey of Hokkaido, 45, 1–23, 1972.
Takayasu, H.: Fractals, Asakura-Shoten, Tokyo, 1986.
Takeuchi, S.: Basic knowledge on studies of fluid inclusions minerals 1: Historical review, classification and formation of fluid inclusions, Journal of the Gemmological Society of Japan, 2, 25–33, 1975.

NPGD
1, 1365–1379, 2014

Tsuchiyama, A., Nakamura, T., Okazaki, T., Uesugi, K., Nakano, T., Sakamoto, K., Akaki, T., Iida, Y., Kadono, T., Jogo, K., and Suzuki, Y.: Three-dimensional structures and elemental distributions of stardust impact tracks using synchrotron microtomography and X-ray fluorescence analysis, Meteorit. Planet. Sci., 44, 1203–1224, 2009.

Witten, T. A. and Sander, L. M.: Diffusion-limited aggregation, Phys. Rev. B, 27, 5686–5697, 1983.

Xie, S., Cheng, Q., Xing, X., Bao, Z., and Chen, Z.: Geochemical multifractal distribution patterns in sediments from ordered streams, Geoderma, 160, 36–46, 2010.

Zheng, D. W., Wen, W., and Tu, K. N.: Reactive wetting- and dewetting-induced diffusion-limited aggregation, Phys. Rev. B, 57, R3719–R3722, 1998.

NPGD
1, 1365–1379, 2014

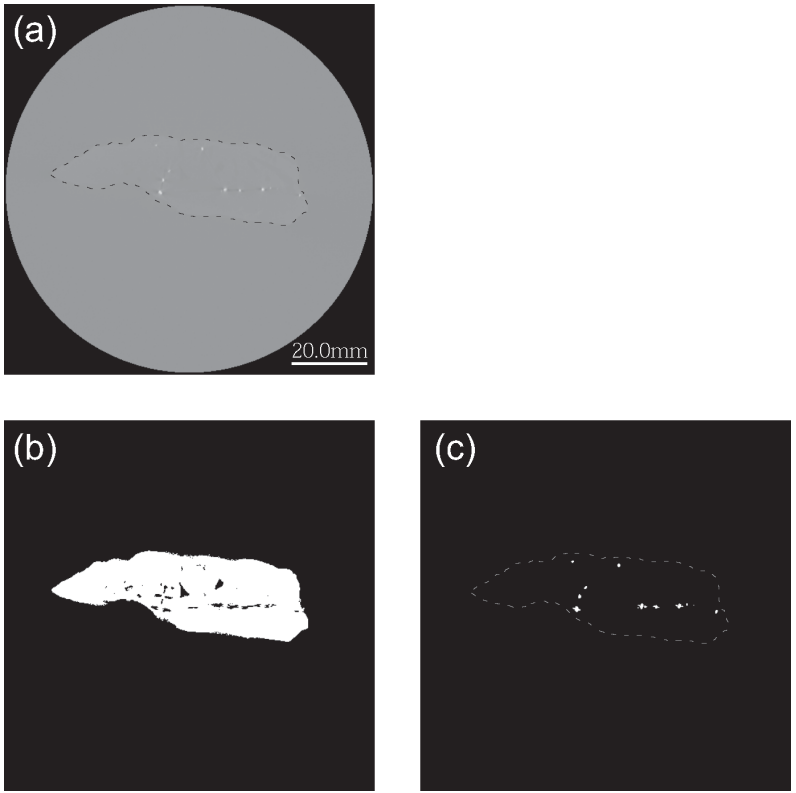

Figure 1. Two-dimensional (2-D) slice image of the San Benito quartz sample obtained with a microfocus X-ray CT system. **(a)** Original grayscale image. The circular dark gray region is the measurable area, the irregular central region is the quartz sample, and the white points are mercury inclusions; **(b)** binatized image of the quartz crystal; and **(c)** binatized image of the mercury inclusions. The quartz area is edged with a dotted line.

NPGD
1, 1365–1379, 2014

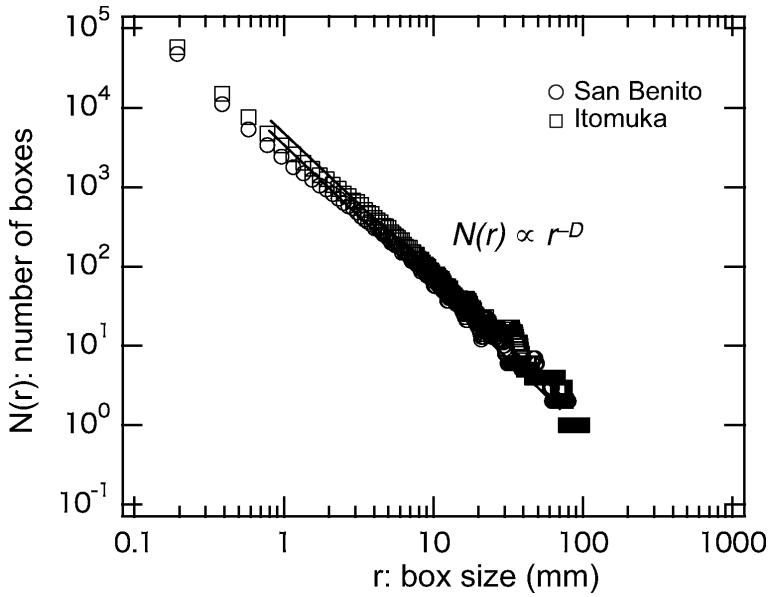

Figure 2. Box counting plot for mercury inclusions in the San Benito and Itomuka quartz samples. To obtain the capacity dimensions, D, only the middle portions of the sequence, from four times the length of the minimal box size to 9/10 of the length of the maximal box size, were analysed to avoid edge effects.

NPGD
1, 1365–1379, 2014

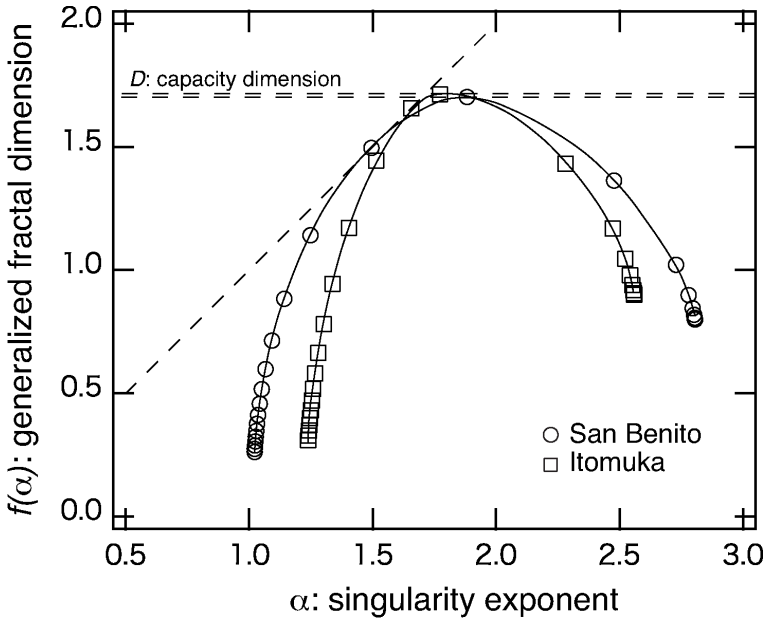

Figure 3. Multifractal spectrum for the mercury inclusions in the San Benito and Itomuka quartz samples. The spectrum is the shape of a downward concave parabola. A wide opening parabola indicates heterogeneous distribution structures in the mercury inclusions.

NPGD
1, 1365–1379, 2014

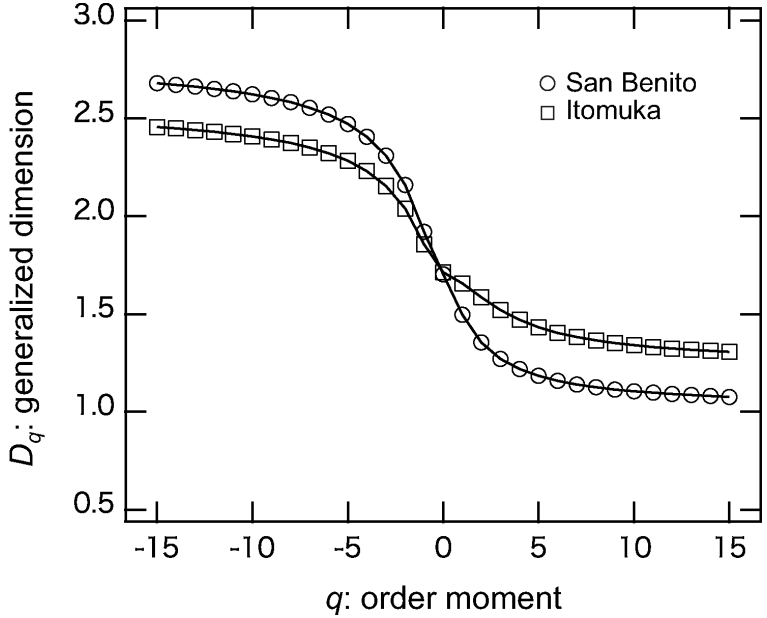

Figure 4. Generalized dimension, D_q, vs. the order moment, q, from $q = -15$ to $q = +15$ for the mercury inclusion distribution in the San Benito and Itomuka quartz samples. The q moment is a measure of the probability density, low-q is low-density and high-q is high-density. The generalized dimension, D_q, indicates the geometrical shape of the mercury inclusion at the q density.

NPGD
1, 1365–1379, 2014